Giant hall photoconductivity in narrow-gapped dirac materials

Song, Justin Chien Wen; Kats, Mikhail A.

2016

Song, J. C. W., & Kats, M. A. (2016). Giant hall photoconductivity in narrow-gapped dirac materials. Nano Letters, 16(12), 7346−7351. doi:10.1021/acs.nanolett.6b02559

https://hdl.handle.net/10356/137991

https://doi.org/10.1021/acs.nanolett.6b02559

Giant Hall photoconductivity in narrow-gapped Dirac materials

Justin C. W. Song[1,2], and Mikhail A. Kats[3,4]
[1] *Institute of High Performance Computing, Agency for Science, Technology, and Research, Singapore 138632*
[2] *Division of Physics and Applied Physics, Nanyang Technological University, Singapore 637371*
[3] *Department of Electrical and Computer Engineering, University of Wisconsin-Madison, Madison WI 53706, USA and*
[4] *Department of Materials Science and Engineering, University of Wisconsin-Madison, Madison WI 53706, USA*

Carrier dynamics acquire a new character in the presence of Bloch-band Berry curvature, which naturally arises in gapped Dirac materials (GDMs). Here we argue that photoresponse in GDMs with small band gaps is dramatically enhanced by Berry curvature. This manifests in a giant Hall photoconductivity when illuminated by circularly polarized light, which can feature appealing characteristics including a saturable behavior. Unlike Hall motion arising from a Lorentz force in a magnetic field, which impedes longitudinal carrier motion, Hall photoconductivity arising from Berry curvature can boost longitudinal carrier transport. In GDMs, this yields helicity-dependent photoresponses in the Hall regime, where photoconductivity is dominated by its Hall component. We find that the induced Hall conductivity per incident irradiance increases by up to six orders of magnitude when moving from the visible regime (with corresponding band gaps) to the far infrared. These results suggest that narrow-gap GDMs are an ideal test-bed for the unique physics that arise in the presence of Berry curvature, and open a new avenue for infrared and terahertz optoelectronics.

Hall motion and its associated Hall conductivity allow currents to flow in a direction transverse to an applied electric field. A signature of time reversal symmetry breaking in electronic systems, this transverse motion has its most dramatic impact in the Hall regime, where the Hall conductivity overwhelms the longitudinal conductivity. As a result, a number of novel behaviors manifest, including deformed current flows [1], and a quantized Hall effect in quantum Hall systems [2].

Recently, gapped Dirac materials (GDMs), characterized by an energy gap 2Δ [3–12], have been found to exhibit a valley Hall effect [6–8, 12–17]. GDMs include transition metal dichalcogenides [11, 12], dual-gated bilayer graphene (BLG) [7–9], and graphene on hexagonal boron nitride heterostructures (G/hBN) with broken A/B sublattice symmetry [3–6]. In these, valley-specific Hall motion arises at zero magnetic field due to Bloch band Berry curvature [13–17]. When the valley carrier population is imbalanced ("valley polarized", see Fig. 1a), a charge Hall effect manifests [12–17]. For example, a small Hall voltage at zero magnetic field was observed in monolayer molybdenum disulfide (MoS_2), a wide-gap GDM with $2\Delta = 1.9\,\mathrm{eV}$ [11], when valley polarized [12]. However, the corresponding Hall conductivities measured in Ref. [12] were small, and the system was far from the Hall regime.

Here we argue that *narrow-gap* GDMs possess a giant photoinduced Hall conductivity $\sigma_{xy}^{\mathrm{pe}}$ when the valley carrier populations are imbalanced (Fig. 1a), which can be achieved via the absorption of light with nonzero helicity [14]. In particular, we find $\sigma_{xy}^{\mathrm{pe}}$ in these narrow-gap GDMs can reach values as high as Ne^2/h, (Fig. 1b) even at small photoexcited carrier densities in a single valley n_{pe}^K. Here N is the spin/flavor degeneracy; in G/hBN, $N = 2$ accounts for spin degeneracy. Narrow-gap GDMs can be realized in G/hBN heterostructures and dual-gated BLG, where the gap can take on small values $2\Delta \lesssim$ tens $\times$ meV [3, 6–10]. In contrast to their wide-gap counterparts, $\sigma_{xy}^{\mathrm{pe}}$ in narrow-gap GDMs exhibit a saturation behavior (Fig. 1b), and can be observed at moderate temperatures (Fig. 3).

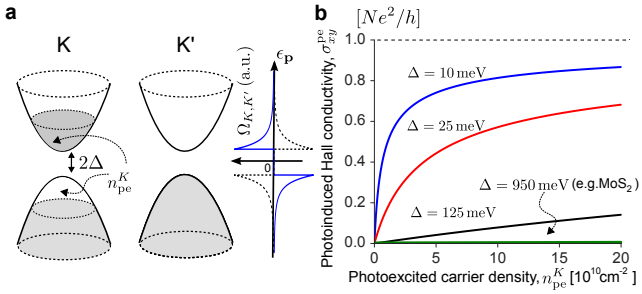

FIG. 1: **a)** Population imbalance between valley K and K' in a gapped Dirac material (GDM) with energy gap 2Δ. The imbalance can be achieved via absorption of circularly polarized light. [inset] Berry curvature $\Omega(\mathbf{p})$ distribution in valley K (blue) and K' (dashed). **b)** Giant photoinduced Hall conductivity, $\sigma_{xy}^{\mathrm{pe}}$, as a function of photoexcited carrier density in a single valley, n_{pe}^K. Note that the green curve, $\Delta = 950\,\mathrm{meV}$ (corresponding to MoS_2), is almost flat in comparison with those for narrow-gap GDMs. Parameters used: $n_{\mathrm{pe}}^{K'} = 0$, initial carrier concentration $n_0 = 0$, and $v = 10^8\,\mathrm{cms}^{-1}$.

Giant values of $\sigma_{xy}^{\mathrm{pe}}$ arise from Berry curvature, $\Omega(\mathbf{p})$, peaking near band edges. In graphene with broken A/B sublattice symmetry [16, 17],

$$\Omega_{\pm}^{\zeta}(\mathbf{p}) = \frac{\pm\hbar^2\zeta v^2\Delta}{2(v^2|\mathbf{p}|^2+\Delta^2)^{3/2}}, \qquad (1)$$

where $\zeta = \pm 1$ denote valley K, K', $\pm$ denote conduc-

tion and valence bands, v is the Dirac particle velocity, and $\mathbf{p}$ are momenta taken relative to the K and the K' points. Importantly, $\Omega(\mathbf{p})$ decays quickly with increasing $|\mathbf{p}|$ (see Fig. 1a), exhibiting a peak height (width) that gets higher (narrower) as Δ decreases. Since $\Omega(\mathbf{p})$ determines the anomalous Hall motion, states close to the band edge dominate the Hall response [17].

Strikingly, $\sigma_{xy}^{\rm pe}$ in narrow-gap GDMs can exceed the longitudinal photoinduced conductivity, $\sigma_{xx}^{\rm pe}$. For GDMs, we find Hall ratios, $\tan\theta_{\rm H} = \sigma_{xy}^{\rm pe}/\sigma_{xx}^{\rm pe}$, as

$$\tan\theta_{\rm H} = \frac{4\mathcal{A}\tilde{n}}{n_{\rm pe}}\left[\frac{\tilde{n}^{1/2}}{\sqrt{\tilde{n}+\frac{n_{\rm pe}^{K'}}{2}}} - \frac{\tilde{n}^{1/2}}{\sqrt{\tilde{n}+\frac{n_{\rm pe}^{K}}{2}}}\right], \quad \mathcal{A} = \frac{e}{4h\tilde{n}\eta}, \tag{2}$$

where $\mathcal{A}$ is the maximal Hall ratio, $n_{\rm pe} = n_{\rm pe}^{K} + n_{\rm pe}^{K'}$ is the total photoexcited carrier density (per spin), $\tilde{n} = \Delta^2/4\pi v^2\hbar^2$ is a gap-dependent characteristic density scale (for $\Delta \neq 0$), η is the mobility of electrons and holes, and h is Planck's constant. When the GDM is maximally polarized, e.g. $n_{\rm pe}^{K} \neq n_{\rm pe}^{K'} = 0$, $\tan\theta_{\rm H}$ approaches $\mathcal{A}$ for small $n_{\rm pe}^{K}$. As a result, $\sigma_{xy}^{\rm pe} > \sigma_{xx}^{\rm pe}$ in narrow-gap GDMs for a fairly large range of mobilities η (shaded region, Fig. 2a), providing access to the Hall regime.

We emphasize that transport arising from Berry curvature in Eq. (1) contrasts starkly with that achieved in a magnetic field, with important qualitative consequences. In a magnetic field, Hall motion arises from a Lorentz force, which impedes the longitudinal motion of charge carriers. In contrast, $\sigma_{xy}^{\rm pe}$ in GDMs resulting from Eq. (1) can enhance longitudinal transport. As we show below, $\sigma_{xy}^{\rm pe}$ suppresses bulk longitudinal photoresistivity (Fig. 2b), and enhances global two-terminal photoconductance (Fig. 2d). This underscores the dichotomy between magneto-transport, and anomalous transport arising from Bloch band Berry curvature, exhibiting new means of manipulating carriers at zero magnetic field.

Hall photoconductivity in GDMs - We begin with the simplified GDM hamiltonian $\mathcal{H} = H_K + H_{K'}$, describing the low energy excitations in graphene with broken A/B sublattice symmetry (e.g. G/hBN), as:

$$H_{K,K'} = \boldsymbol{\tau}\cdot\mathbf{d}(\mathbf{p}), \quad \mathbf{d}(\mathbf{p}) = (vp_x, \zeta vp_y, \Delta) \tag{3}$$

where $H_K, H_{K'}$ describe electronic states in the valleys close to the K and K' points, and $\boldsymbol{\tau} = \tau_x\hat{\mathbf{x}} + \tau_y\hat{\mathbf{y}} + \tau_z\hat{\mathbf{z}}$. Here $\tau_{x,y,z}$ are the Pauli matrices operating on the sub-lattices, and $\mathbf{p} = (p_x, p_y)$ lies in x-y (in-plane). The eigenfunctions of Eq. (3) are the pseudospinors: $|\psi_+(\mathbf{p})\rangle = (\cos\frac{\theta}{2}e^{-\zeta i\phi}, \sin\frac{\theta}{2})$, and $|\psi_-(\mathbf{p})\rangle = (\sin\frac{\theta}{2}e^{-\zeta i\phi}, -\cos\frac{\theta}{2})$ [18] with energy eigenvalues $\varepsilon_{\mathbf{p}}^{\pm} = \pm\sqrt{v^2|\mathbf{p}|^2 + \Delta^2}$, where $\tan\theta = v|\mathbf{p}|/\Delta$, and $\tan\phi = p_y/p_x$. Here v is the relativistic velocity of Dirac particles when particle energy $\varepsilon_{\mathbf{p}} \gg \Delta$. We note that Eq. (3) captures the essential long-wavelength physics of a broad range of GDMs. In particular, a similar analysis also applies for dual-gated BLG (see SOI).

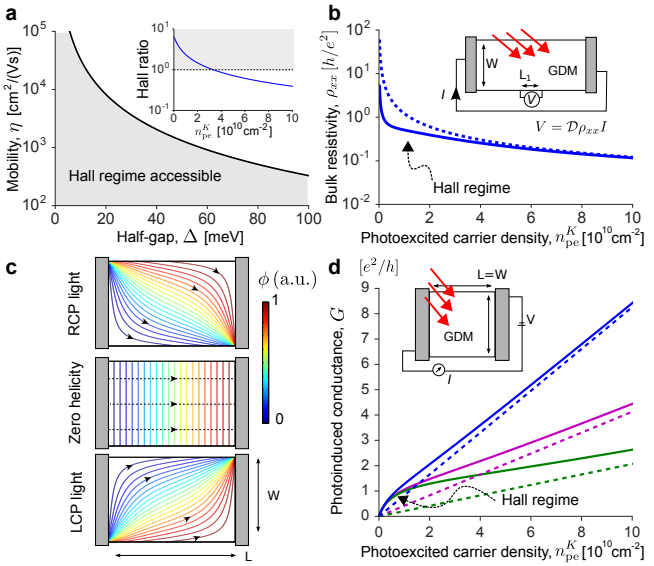

FIG. 2: **a)** The Hall regime in GDMs can be accessed when $\sigma_{xy}^{\rm pe} > \sigma_{xx}^{\rm pe}$, indicated by the shaded area. The black line corresponds to $\mathcal{A} = 1$ [Eq. (2)], where $\mathcal{A}$ is the maximal Hall ratio. (inset) The Hall ratio can be controlled by $n_{\rm pe}^K$. Here we plot Hall ratio for $\Delta = 10\,$meV and $\eta = 10^4\,{\rm cm}^2/({\rm Vs})$, with shaded region indicating the Hall regime. **b)** Longitudinal (bulk) photoresistivity, $\rho_{xx} = V/(I\mathcal{D})$, experiences a large suppression in the Hall regime. Parameters used are the same as in the inset to (a), and $\mathcal{D} = L_1/W$ is a geometrical factor. **c)** Equipotentials in a finite rectangular geometry (length and width, L and W) are deformed in the presence of large $\sigma_{xy}^{\rm pe}$, shown for $\sigma_{xy}/\sigma_{xx} = -10, 0, -10$ respectively. Current flow lines (black arrows) are normal to equipotentials when $\sigma_{xy}/\sigma_{xx} = 0$ (center panel). In contrast, current flow lines follow the equipotentials resulting from the absorption of LCP/RCP light in GDMs (top/bottom panels, see text). **d)** Enhanced two terminal photoconductance, $G = I/V$, for a square geometry $L = W$ (inset) exhibiting a non-linear $n_{\rm pe}^K$ dependence. Here $\eta = 1,\ 0.5,\ 0.25\times10^4\,{\rm cm}^2/{\rm Vs}$ for blue, magenta, and green curves respectively, with parameters same as (a) inset. Dashed lines correspond to G with $\sigma_{xy}^{\rm pe} = 0$. The above analysis is valid in the semiclassical limit, where the mean free path is larger than the electron wavelength.

Electrons wavepackets formed out of the Bloch wavefunctions with $|\psi_\pm(\mathbf{p})\rangle$ possess an intrinsic angular momentum that skews the electron velocity, $\dot{\mathbf{x}}_{\mathbf{p}}$ as [16]

$$\dot{\mathbf{x}}_{\mathbf{p}} = \frac{\partial\varepsilon_{\mathbf{p}}}{\partial\mathbf{p}} + \mathbf{v}_a, \quad \mathbf{v}_a = \frac{1}{\hbar}\dot{\mathbf{p}}\times\Omega_\zeta^{\pm}(\mathbf{p}), \quad \dot{\mathbf{p}} = q\mathbf{E}, \tag{4}$$

where $\partial\varepsilon_{\mathbf{p}}/\partial\mathbf{p}$ is the group velocity, and q is the carrier charge. In the presence of anomalous velocity, $\mathbf{v}_a$, $\dot{\mathbf{x}}_{\mathbf{p}}$ is no longer parallel to its momentum. As a result, Bloch electrons in each of the valleys experience a Hall effect even without the application of a magnetic field [16, 19], albeit of opposite sign. In our analysis below, we do not consider extrinsic disorder-related mechanisms which can contribute to the anomalous Hall effect [19]. Instead, we concentrate on the intrinsic mechanism in GDMs, arising

from $\mathbf{v}_a$, to clearly illustrate the features in the photo-induced Hall regime.

We proceed by writing the current density $\mathbf{j} = q\sum_{\mathbf{p},\pm,\zeta} f^{\zeta}_{\pm}(\mathbf{p})\dot{\mathbf{x}}$, yielding $j_i = \sigma_{ij}E_j$. Here $f^{\zeta}_{\pm}(\mathbf{p})$ is the distribution function with $\pm,\zeta$ denoting conduction/valence bands and valley K/K' respectively. Focussing on the Hall conductivity, and using Eq. (4), we have

$$\sigma_{xy} = \frac{Ne^2}{h}\Big[\sum_{\mathbf{p},\pm} f^{K}_{\pm}(\mathbf{p})\Omega^{K}_{\pm}(\mathbf{p}) + \sum_{\mathbf{p},\pm} f^{K'}_{\pm}(\mathbf{p})\Omega^{K'}_{\pm}(\mathbf{p})\Big]. \quad (5)$$

We note that at zero magnetic field, $\Omega^{K'}_{\pm} = -\Omega^{K}_{\pm}$ [16]. As a result, at equilibrium, the distribution functions $f_{K,\pm} = f_{K',\pm}$, giving equal carrier densities in each of the valleys, $n_K = n_{K'}$, and a σ_{xy} that vanishes. However, when pushed out of equilibrium, $f_K \neq f_{K'}$, yielding $\sigma_{xy} \neq 0$.

Assuming fast relaxation of the photoexcited carriers to the band-edge [20, 21], the steady-state carrier population in each of the valleys can be modeled by distribution functions with split electron and hole quasi-Fermi levels:

$$f^{\zeta}_{+}(\mathbf{p}) = [1+e^{\beta(\varepsilon^{+}_{\mathbf{p}}-\mu_{\mathrm{el},\zeta})}]^{-1}, \quad f^{\zeta}_{-}(\mathbf{p}) = [1+e^{\beta(\varepsilon^{-}_{\mathbf{p}}-\mu_{\mathrm{h},\zeta})}]^{-1}, \quad (6)$$

where $\mu_{\mathrm{el},\zeta} \neq \mu_{\mathrm{h},\zeta}$ are the electron and hole quasi-fermi levels induced by photoexcitation, and $\beta = 1/k_BT$ with T the temperature.

We first examine the degenerate limit, $\mu_{\mathrm{el,h}}, \Delta \gg k_BT$. Writing the initial carrier density per flavor *before* irradiation as $n_K = n_{K'} = n_0$, and using Eq. (5) and Eq. (6), we obtain a photo-induced Hall conductivity as

$$\sigma^{\mathrm{pe}}_{xy} = \frac{Ne^2}{h}\Big[\mathcal{F}_K(n^{K}_{\mathrm{pe}}/2) + \mathcal{F}_{K'}(n^{K'}_{\mathrm{pe}}/2)\Big],$$
$$\mathcal{F}_{\zeta}(x) = \frac{\zeta}{2}\Big(1 - \Big[\frac{\tilde{n}^{1/2}}{\sqrt{\tilde{n}+n_0+x}} + \frac{\tilde{n}^{1/2}}{\sqrt{\tilde{n}+x}}\Big]\Big), \quad (7)$$

where $\mathcal{F}_{\zeta}$ with $\zeta = \pm 1$ denote contributions of the K and K' valleys respectively, and $\tilde{n} = \Delta^2/4\pi v^2\hbar^2$ is the characteristic density. Here we noted that the photoexcited electron and hole densities can be written as $n_{\mathrm{el,h}} = \mu^2_{\mathrm{el,h}}/4\pi\hbar^2v^2 - \tilde{n}$, and neglected finite T corrections by setting $T = 0$ (see below for discussion of temperature dependence). We have also taken $n^{K}_{\mathrm{el}} = n^{K}_{\mathrm{h}} = n^{K}_{\mathrm{pe}}/2$, and $n^{K'}_{\mathrm{el}} = n^{K'}_{\mathrm{h}} = n^{K'}_{\mathrm{pe}}/2$, where n_{el} and n_{h} are the photoexcited electron and hole populations in the K, K' valleys.

Crucially, $\tilde{n} = \Delta^2/4\pi v^2\hbar^2$ determines the characteristic scale with which valley population imbalance, $\delta n = n^{K}_{\mathrm{pe}} - n^{K'}_{\mathrm{pe}}$, yields appreciable σ_{xy}. For example, for $\Delta = 10\,\mathrm{meV}$, we find $\tilde{n} = 1.8\times10^9\,\mathrm{cm}^{-2}$ (setting $v = 10^8\,\mathrm{cm\,s}^{-1}$). As a result in narrow-gap GDMs, only small imbalance δn is needed to achieve sizable $\sigma^{\mathrm{pe}}_{xy}$. This unusual behavior is a result of states close to the band edge contributing the maximum amount to Hall conductivity in GDMs [17] (Fig. 1a).

Taking $n_0 = 0$, we find a giant photoinduced Hall conductivity $\sigma^{\mathrm{pe}}_{xy}$, shown in Fig. 1b. Here we have set

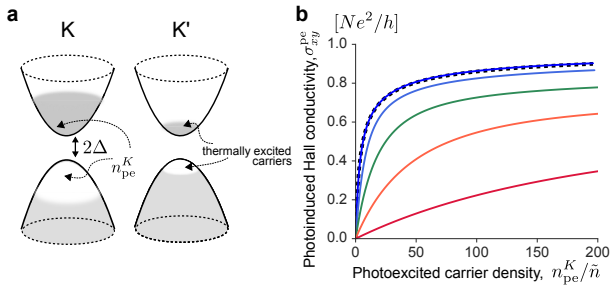

FIG. 3: a) At finite temperature, both K and K' possess thermally excited carriers. b) Photoinduced Hall conductivity, $\sigma^{\mathrm{pe}}_{xy}$, decreases as a function of temperature. Shown are plots obtained numerically integrating Eq. (5) for $k_BT/\Delta = 0.1, 0.5, 1, 2, 5$ (top to bottom); dashed curve is Eq. (7) where $T = 0$ and we have set the chemical potential before photoexciation to be in the gap.

$n^{K'}_{\mathrm{pe}} = 0$, with only carriers in the K valley excited. The maximum achievable $\sigma^{\mathrm{pe}}_{xy}$ is Ne^2/h as shown in Eq. (7), when $n^{K}_{\mathrm{pe}} \gg \tilde{n}$. Since $\tilde{n}$ can be small in GDMs with narrow gaps, this saturation behavior can be easily accessed. An opposite sign of Hall conductivity is obtained when instead K' carriers are photoexcited, e.g., by absorption of light with opposite helicity. $\sigma^{\mathrm{pe}}_{xy}$ can be directly measured in a four-terminal Hall-type geometry, as in Ref. [12].

Interestingly, $\sigma^{\mathrm{pe}}_{xy}$ [Eq. (7)] can be tuned by n_0 (and gate) exhibiting an *even* behavior in n_0 and reaching a maximum when $n_0 = 0$ (charge neutrality). Due to its even-ness, $\sigma^{\mathrm{pe}}_{xy}$ is robust to density inhomogeneity. This contrasts with that of ordinary Hall conductivity, which changes sign with carrier type, and vanishes for charge-neutral systems.

At finite temperature, both K and K' valleys possess thermally excited carriers (Fig. 3a). We plot the temperature dependence of $\sigma^{\mathrm{pe}}_{xy}$ in Fig. 3b. Here we have integrated Eq. (5) numerically using Eq. (6). Photoexcited carrier density was also obtained numerically via $n^{K,K'}_{\mathrm{pe}} = \sum_{\mathbf{p}} f_{\zeta,\pm}(\mathbf{p})$. In our plots, we characterized temperature dependence via the dimensionless parameter k_BT/Δ. As shown in Fig. 3b, $\sigma^{\mathrm{pe}}_{xy}$ *decreases* as temperature increases. In particular, temperature dependence of $\sigma^{\mathrm{pe}}_{xy}$ becomes pronounced only when $k_BT/\Delta \gtrsim 1$. This arises since $\Omega(\mathbf{p})$ in Eq. (1) only varies appreciably when $v|\mathbf{p}| \sim \Delta$. As T is increased, the typical square-root type dependence of $\sigma^{\mathrm{pe}}_{xy}$ on n^{K}_{pe} straightens out, approaching a nearly linear dependence for large temperatures (see e.g. $k_BT/\Delta = 5$ in Fig. 3b). In plotting Fig. 3b, we have chosen the chemical potential before photoexcitation to lie inside the gap, so that $n_0 = 0$ for $T = 0$.

Photoinduced Hall regime - To give a sense of scale, it is useful to compare $\sigma^{\mathrm{pe}}_{xy}$ to the longitudinal photoconductivity, $\sigma^{\mathrm{pe}}_{xx}$. We use a simple model for $\sigma^{\mathrm{pe}}_{xx} = eN\eta n_{\mathrm{pe}}$, where $n_{\mathrm{pe}} = n^{K}_{\mathrm{pe}} + n^{K'}_{\mathrm{pe}}$ is the photoex-

cited carrier density (per flavor/spin N), and $n_0 = 0$. Here η is the mobility of electrons and holes. Taking the ratio of $\sigma^{\rm pe}_{xy}$ and $\sigma^{\rm pe}_{xx}$ in Eq. (7), we obtain the Hall ratio in Eq. (2). Setting the maximal Hall ratio to unity, $\mathcal{A} = 1$, we obtain the black curve in Fig. 2a. This indicates that a large range of mobilities yield $\sigma^{\rm pe}_{xy} > \sigma^{\rm pe}_{xx}$, see shaded region. The Hall ratio can be controlled via the photoexcited carrier density, and is maximized at small values of $n^K_{\rm pe}$ (Fig. 2a inset). We note that when $\Delta = 0$, the terms inside the brackets of Eq. (2) vanish.

For G/hBN, gap sizes $2\Delta \approx 10 - 40\,{\rm meV}$ and mobility that ranged $\eta \approx 5 \times 10^3 - 10^5\,{\rm cm}^{-2}/({\rm Vs})$ have been inferred [3–6]. We anticipate that for the smallest gap sizes, $\Delta \approx$ few $\times$ meV [3–6], and the lowest mobilities Hall ratios of order ten may be obtained.

Access to the photoinduced Hall regime invites a comparison with magneto-transport of charge carriers. In the latter, aside from yielding a Hall conductivity, the Lorentz force due to the presence of a magnetic field impedes the longitudinal motion of charge carriers. For example, for a single carrier type in a homogeneous system, a simple Drude model yields bulk σ_{xx} that is suppressed with increasing magnetic field; it also yields a longitudinal resistivity that is unchanged with magnetic field [1].

In contrast, in the photoinduced Hall regime in GDMs, we find that (bulk) longitudinal *photoresistivity*, ρ_{xx}, becomes suppressed. Writing $\mathbf{j}(\mathbf{r}) = \underline{\underline{\boldsymbol{\sigma}}}\,[-\boldsymbol{\nabla}\phi(\mathbf{r})]$, and inverting $\underline{\underline{\boldsymbol{\sigma}}}$, we obtain

$$\rho_{xx} = \frac{\sigma_{xx}}{\sigma^2_{xx} + \sigma^2_{xy}} = \frac{\mathcal{C}}{\sigma^{\rm pe}_{xx}}, \quad \mathcal{C} = \frac{1}{1 + (\tan\theta_H)^2}, \qquad (8)$$

where we have set $\sigma_{xx} = \sigma^{\rm pe}_{xx}$ to accentuate the contribution of the photoexcited carriers. In the Hall regime in Fig. 2b, we find $\mathcal{C} \ll 1$ leading to a suppressed ρ_{xx} (solid line) as compared with $\sigma_{xy} = 0$ (dashed line). For example, $\Delta = 10\,{\rm meV}$ and $\eta = 10^4\,{\rm cm}^2/(Vs)$, we find $\mathcal{C} \approx 0.1$ yielding a large suppression. This can be measured via non-invasive local probes in long Hall bars (Fig. 2b inset), so that the probes are far away from distorted fields near contacts.

The dichotomy between magneto-transport and the photoinduced Hall regime in GDMs arises from the differences in the origin of their Hall motion. In magneto-transport, the Lorentz force alters the force balance on charge carriers, and diverts momentum transversely; this impedes longitudinal motion. In the photoinduced Hall regime, $\mathbf{v}_a$ appears in addition to longitudinal flow in Eq. (4), and does not obstruct longitudinal motion since it does not enter into the force balance. As a result, for $\mathbf{j}$ flowing along equipotential lines in the photoinduced Hall regime, smaller electric fields are sustained giving a suppressed ρ_{xx} in Eq. (8) [27].

The Hall regime can also change the "global" pattern of current flow [1, 22–24], as shown in Fig. 2c. Here we have contrasted $\phi(\mathbf{r})$ for $|\sigma_{xy}| \gg \sigma_{xx}$ (top/bottom panels) with $\sigma_{xy} = 0$ [28]. In the former case, current flow is non-uniform. Indeed, when the sign of σ_{xy} is changed, e.g. by changing between left- (LCP) and right- (RCP) hand circularly polarized irradiation, the location of "hot-spot" regions of largest electric field can switch.

As a result, the two-terminal conductance $G = I/V$, acquires a sensitivity to σ_{xy} [22–25]. Here $I = \int_0^W j_y dx$, and $V = \phi_{\rm source} - \phi_{\rm drain}$ (Fig. 2d inset). In an arbitrary geometry, G can be obtained numerically [24, 25]. However, for a conducting square $L = W$ [22, 23],

$$G = \left[(\sigma_{xy})^2 + (\sigma_{xx})^2\right]^{1/2} = \sigma^{\rm pe}_{xy}\sqrt{1 + 1/(\tan\theta_{\rm H})^2}, \quad (9)$$

where in the last line we have set $\sigma_{xx} = \sigma^{\rm pe}_{xx}$, and $\sigma_{xy} = \sigma^{\rm pe}_{xy}$ (realizable for $n_0 = 0$ and $k_B T/\Delta \ll 1$). For brevity, we focus on this geometry. Using $\sigma_{xy} = \sigma^{\rm pe}_{xy}$ obtained for GDMs in Eq. (7), we obtain the two-terminal photoconductance in Fig. 2d.

In the Hall regime, $\sigma^{\rm pe}_{xy}$ provides the dominant contribution to two-terminal conductance G (Fig. 2d), which displays a non-linear $n^K_{\rm pe}$ dependence that resembles that of $\sigma^{\rm pe}_{xy}$ in Fig. 1b. This is particularly pronounced at low $n^K_{\rm pe}$, where G displays a "universal" profile that is insensitive to mobility, boosting G. At large $n^K_{\rm pe} \gg \tilde{n}$, the Hall ratio diminishes, and G loses its sensitivity to the helicity of the incident light (dashed line). In that regime, σ_{xx} dominates G.

The boost to G in the photoinduced Hall regime in GDMs contrasts with that of magneto-transport. In the latter, G decreases in the presence of a magnetic field in the semiclassical limit [29]. The dependence of G on the degree of circular polarization in the former, and the boost to longitudinal carrier motion [Eq. (2), Eq. (9)], are striking signatures of the unique Hall regime accessed in narrow-gap GDMs.

Enhanced valley-imbalance rate - We now turn to valley-imbalance, $\delta n = n^K_{\rm pe} - n^{K'}_{\rm pe}$, induced by the absorption of circularly polarized light [12, 14]. As we argue below, narrow-gap GDMs can experience an enhanced rate of imbalance between the valleys $d\delta n/dt$ (as compared with their wide-gap GDM counterparts) when irradiated by light of non-zero helicity. We model the rate of electron-hole pair creation in each valley, $W_{K(K')}$, via Fermi's golden rule

$$W_{K(K')} = \frac{2\pi}{\hbar}\sum_{\mathbf{k}} |M^{K(K')}_{\mathbf{k}}|^2 \delta(\varepsilon_{\mathbf{k}} - \hbar\omega/2), \qquad (10)$$

where the matrix elements are $M^{K(K')}_{\mathbf{k}} = \frac{iev}{2\omega}\langle\psi_+|E_x\tau_x + \zeta E_y\tau_y|\psi_-\rangle$ [26], and the incident light electric field is $\mathbf{E}$ with photon energy $\hbar\omega \geq 2\Delta$. Eq. (10) arises from writting $\mathbf{p} \to \mathbf{p} - e\mathbf{A}/c$ in Eq. (3), with the vector potential satisfying $\mathbf{A} = \frac{ic}{\omega}\mathbf{E}$.

Using the pseudo-spinor states $|\psi_\pm(\mathbf{p})\rangle$ for GDMs given above, we have $\langle\psi_+|\tau_x|\psi_-\rangle = \sin^2\frac{\theta}{2}e^{-i\zeta\phi} -$

$\cos^2\frac{\theta}{2}e^{i\zeta\phi}$, $\langle\psi_+|\tau_y|\psi_-\rangle = i\big(\sin^2\frac{\theta}{2}e^{-i\zeta\phi} + \cos^2\frac{\theta}{2}e^{i\zeta\phi}\big)$. For normally incident circularly polarized light, $\mathbf{E} = |\mathbf{E}|(\hat{\mathbf{x}} + id\hat{\mathbf{y}})/\sqrt{2}$, where $d = \pm 1$ for LCP and RCP polarizations, and gives the rate (per spin N)

$$W_K^d = W_0\big(\frac{2\Delta}{\hbar\omega} + d\big)^2, \quad W_{K'}^d = W_0\big(\frac{2\Delta}{\hbar\omega} - d\big)^2, \quad (11)$$

where $W_0 = e^2|\mathbf{E}|^2/(16\hbar^2\omega)$, and $\hbar\omega \geq 2\Delta$. Eq. (11) describes valley selective electron-hole transitions resulting from the absorption of light with non-zero helicity, in agreement with Ref. [14].

Importantly, the K and K' asymmetry in Eq. (11) yields a valley population imbalance rate (per spin N)

$$\frac{d\delta n}{dt}\Big|^d = 2\big(W_K^d - W_{K'}^d\big) = d\frac{e^2|\mathbf{E}|^2}{\hbar^2\omega}\frac{\Delta}{\hbar\omega}, \quad (12)$$

where $\hbar\omega \geq 2\Delta$, and the factor of 2 in the second line accounts for both electron and hole populations. The rate $d\delta n/dt$ grows quickly for decreasing ω, and reaches a maximum at $\hbar\omega = 2\Delta$, yielding $\max(d\delta n/dt) = e^2|\mathbf{E}|^2/4\hbar\Delta$; $d\delta n/dt$ vanishes for $\hbar\omega < 2\Delta$ As a result, large K/K' carrier density imbalance rates, $d\delta n/dt$, can be achieved for narrow-gap GDMs when irradiated with circularly polarized light on resonance with the gap.

Combining the enhancements for narrow-gap GDMs in both Eq. (7) and Eq. (12) yields a large value of $\sigma_{xy}^{\rm pe}$ per incident light irradiance, $\mathcal{P}_{\rm in} = c|\mathbf{E}|^2/(4\pi)$. This is particularly striking in the *low* irradiance regime where we can expand Eq. (7) to lowest order in δn. This gives a *linearized* photoinduced Hall conductivity, $\tilde{\sigma}_{xy}^{\rm pe}$, as

$$\tilde{\sigma}_{xy}^{\rm pe} = d\frac{S_0\mathcal{P}_{\rm in}}{(\hbar\omega)^2\Delta}, \quad S_0 = \frac{4Ne^2}{h}\frac{\alpha\pi^2\hbar^2v^2}{\gamma}, \quad (13)$$

where $\alpha = e^2/\hbar c$ is the fine structure constant, and we have estimated $\delta n = \gamma^{-1}(d\delta n/dt)\big|^d$, with γ the net relaxation rate which may include electron-hole recombination as well as inter-valley scattering; we have taken doping density $n_0 = 0$. For incident LCP/RCP light with frequency above the gap, $\tilde{\sigma}_{xy}^{\rm pe}/\mathcal{P}_{\rm in}$ scales as $[(\hbar\omega)^2\Delta]^{-1}$, reaching a maximum for $\hbar\omega = 2\Delta$ where it scales as $\tilde{\sigma}_{xy}^{\rm pe}/\mathcal{P}_{\rm in} \propto 1/\Delta^3$. As a result, we find $\tilde{\sigma}_{xy}^{\rm pe}/\mathcal{P}_{\rm in}$ can vary over six orders of magnitude from $\Delta \approx 1\,\text{eV}$ (e.g. MoS_2) to $\Delta \approx 10$meV (e.g. G/hBN). This large scaling clearly underscores how the effect of Berry curvature on photoresponse is maximized for narrow-gap GDMs.

In conclusion, GDMs with small gaps are an ideal system in which to probe and utilize the anomalous motion of carriers resulting from the presence of Berry curvature. The giant Hall photoconductivity in such narrow-gap GDMs results in unique phenomena that can be observed at room temperature, including access to the Hall regime in the absence of a magnetic field. Unlike in the case of conventional Hall effect due to a magnetic field, which impedes longitudinal motion, Hall photoconductivity arising from Berry curvature in GDMs boosts it. This demonstrates the contrast between conventional magneto-transport, and Berry curvature induced transport, and unveils new means of controlling carrier transport at zero field.

The implications for far-infrared and terahertz optoelectronics are intriguing. While the Hall photoresponse of GDMs with large gaps – e.g. molybdenum disulfide (MoS_2) – is likely too small for practical optoelectronics applications, the corresponding photoresponse in small-gap GDMs, such as graphene on hexagonal boron nitride (G/hBN), can be significant. In a simple two-terminal photoconductor, the anomalous conductance boost can provide additional sensitivity at low input powers. Combining such a valley Hall photoconducting detector with a traditional photodetector can yield a measurement of the degree of circular polarization of an incident wave, without the need for wave-plates or other polarization-conversion schemes. Furthermore, direct measurements of the Hall photocurrent in a four-terminal Hall-bar geometry may yield a photoconductor-like detection mechanism that exhibits zero net dark current, even in the presence of a large voltage bias. This unusual characteristic, when combined with the giant Hall photoconductivity of narrow-gap GDMs, provides a new route toward high-sensitivity long-wavelength detectors.

We are grateful to Valla Fatemi and Alex Frenzel for helpful discussions, as well as a critical reading of our manuscript. This work was supported by the Singapore National Research Foundation (NRF) under NRF fellowship award NRF-NRFF2016-05 (J.C.W.S.), and by startup funds from UW-Madison (M.A.K.)

[1] Davies, J. H., *The physics of low-dimensional semiconductors*, Cambridge University Press, Cambridge, 1997.
[2] von Klitzing, K., *Rev. Mod. Phys.* **1986**, 58, 519.
[3] Hunt, B.; et al., *Science* **2013**, 340, 1427.
[4] Woods, C. R.; et al., *Nat. Phys.* **2014**, 10, 451.
[5] Chen, Z.-G; et al., *Nat. Comm.* **2014**, 5, 4461.
[6] Gorbachev, R.V.; et al., *Science* **2014**, 346, 448.
[7] Sui, M.; et al., *Nat. Phys.* **2015**, 11, 1027.
[8] Shimazaki, Y.; et al., *Nat. Phys.* **2015**, 11, 1032.
[9] Zhang, Y.; et al., *Nature* **2009**, 459, 820.
[10] Ju, L.; et al., *Nature* **2015**, 520, 650.
[11] Mak, K. F.; et al.; *Phys. Rev. Lett.* **2012**, 105, 136805.
[12] Mak, K. F.; McGill, K. L.; Park, J.; McEuen, P. L.; *Science* **2014**, 344, 1489.
[13] Xiao, D.; Yao, W.; Niu, Q., *Phys. Rev. Lett.* **2007**, 99, 236909.
[14] Yao, W.; Xiao, D.; Niu, Q., *Phys. Rev. B* **2008**, 77, 235406.
[15] Xiao, D.; Liu, G.B.; Feng, W.; Xu, X.; Yao, W., *Phys. Rev. Lett.* **2012**, 108, 196802.
[16] Xiao, D.; Meng, M.-C.; Niu, Q., *Rev. Mod. Phys.* **2010**, 82, 1959.
[17] Lensky, Y. D.; Song, J. C. W.; Samutpraphoot, P.; Levitov, L. S., *Phys. Rev. Lett.* **2015**, 114, 256601.

[18] Bernevig, B. A.; Hughes, T. L., *Topological Insulators and Topological Superconductors*, Princeton University Press, Princeton, 2013.

[19] Nagaosa N.; Sinova, J.; Onoda, S.; Mac- Donald A.H.; Ong, N. P., *Rev. Mod. Phys.* **2010**, 82, 1539.

[20] Gierz, I.; et al., *Nat. Mater.* **2013**, 12, 1119.

[21] Johannsen, J. C.; et al., *Phys. Rev. Lett.* **2013**, 111, 027403.

[22] Lippmann, H. J.; Kuhrt, R.; *Z. Naturf* **1958**, 13, 462.

[23] Jensen, H. H.; Smith, H., *J. Phys. C: Solid State Phys.* **1972**, 5, 2867.

[24] Abanin, D. A.; Levitov, L. S., *Phys. Rev. B* **2008**, 78, 035416.

[25] Rendell, R. W.; Girvin, S. M.; *Phys. Rev. B* **23**, 6610.

[26] M. I. Katsnelson, *Graphene: Carbon in two dimensions*, Cambridge University Press, Cambridge (2012).

[27] We note that $\sigma_{xx}^{\mathrm{pe}}$ is unaffected by $\mathbf{v}_a$ in the photoinduced Hall regime. This contrasts with a single carrier Drude model in a magnetic field, which exhibits a suppressed σ_{xx} and constant ρ_{xx}. This displays the duality between Berry curvature effects and magneto-transport.

[28] Here we have solved current continuity $\boldsymbol{\nabla}\cdot\mathbf{j}=0$ in steady state, with boundary conditions $\phi(\mathbf{r})\big|_{\mathbf{r}=c_k}$ = const and $\mathbf{j}(\mathbf{r})\cdot\hat{\mathbf{n}}\big|_{\mathbf{r}=b_k}=0$, where c_k and b_k label boundaries with metallic contacts (e.g., source and drain) and without metallic contacts (e.g., sample boundaries) respectively. Here $\hat{\mathbf{n}}$ is the unit normal vector to the boundary, and we have used uniform σ.

[29] This can be seen by writing for a single carrier Drude model: $\sigma_{xx}=\sigma_0/(1+\omega_c^2\tau^2)$, and $\sigma_{xy}=\sigma_0\omega_c\tau/(1+\omega_c^2\tau^2)$, and substituting into Eq. (9). Here σ_0 is longitudinal conductivity at zero magnetic field, ω_c is the cyclotron frequency, and τ is the scattering time.

Supplementary Information to "Giant Hall photoconductivity in narrow-gapped Dirac materials"

Justin C. W. Song[1,2], and Mikhail A. Kats[3,4]
[1] *Institute of High Performance Computing, Agency for Science, Technology, and Research, Singapore 138632*
[2] *Division of Physics and Applied Physics, Nanyang Technological University, Singapore 637371*
[3] *Department of Electrical and Computer Engineering, University of Wisconsin-Madison, Madison WI 53706, USA and*
[4] *Department of Materials Science and Engineering, University of Wisconsin-Madison, Madison WI 53706, USA*

In this supplement we discuss Berry curvature and Hall photoconductivity in dual-gated Bilayer graphene which can host an energy gap tunable by an inter-layer electric potential.

$\sigma_{xy}^{\rm pe}$ in dual-gated bilayer graphene

For small inter-layer biases, the low energy hamiltonian of dual-gated bilayer graphene can be approximated in the compact fashion similar to Eq. (3) of the main text as $H_{K,K'} = \mathbf{d}(\mathbf{p})\cdot\boldsymbol{\tau}$ but with $\mathbf{d}(\mathbf{p})$ written as [1–3]

$$\mathbf{d}(\mathbf{p}) = (v^2[p_x^2 - p_y^2]/\gamma_1,\, 2\zeta v^2 p_x p_y/\gamma_1,\, \Delta), \tag{S-1}$$

where γ_1 is the nearest-interlayer-neighbor hopping amplitude, and $\zeta = \pm 1$ for electron in the K and K' valleys as in the main text. This hamiltonian is valid so long as $\gamma_1 \gg \Delta$, and $v|\mathbf{p}| \gg \Delta$. Since $\gamma_1 \approx 0.38\,\text{eV}$ [4], and $2\Delta \approx$ few $- 100\,\text{meV}$ have been reported [5–8], Eq. (S-1) captures the low-energy physics of dual-gated bilayer graphene in the density range $n \gg \tilde{n}$ we are interested in. Here $\boldsymbol{\tau} = \tau_x\hat{\mathbf{x}} + \tau_y\hat{\mathbf{y}} + \tau_z\hat{\mathbf{z}}$, where $\tau_{x,y,z}$ are the Pauli matrices which act on the A/B sub-lattice space in alternate layers [i.e. the spinor is written as $(\psi_{B,\text{top}}, \psi_{A,\text{bottom}})$]. Diagonalizing Eq. (S-1) yields energies

$$\varepsilon_\pm = \pm\sqrt{v^4|\mathbf{p}|^4/\gamma_1^2 + \Delta^2}. \tag{S-2}$$

The Berry curvature for dual-gated bilayer graphene in Eq. (S-1) can be written as [2, 3, 6]

$$\Omega_\pm^\zeta = \pm\frac{2\zeta\hbar^2\Delta\gamma_1 v^4|\mathbf{p}|^2}{(v^4|\mathbf{p}|^4 + \gamma_1^2\Delta^2)^{3/2}} \tag{S-3}$$

Interestingly, while peaked near the band edges, $\Omega(\mathbf{p})$ for dual-gated BLG vanishes for $\mathbf{p} = 0$, in contrast to Eq. (1) in the main text for gapped single layer graphene.

Following the same procedure as the main text, we can write the initial carrier density per spin *before* irradiation as $n_K = n_{K'} = n_0$. Using Eq. (5) and Eq. (6) of the main text, we obtain a photo-induced Hall conductivity in dual-gated BLG as

$$\sigma_{xy}^{\rm pe} = \frac{Ne^2}{h}\Big[\mathcal{G}_K(n_{\rm pe}^K/2) + \mathcal{G}_{K'}(n_{\rm pe}^{K'}/2)\Big],$$
$$\mathcal{G}_\zeta(x) = \zeta\left(1 - \Big[\frac{(\tilde{n}n_1)^{1/2}}{\sqrt{x^2+\tilde{n}n_1}} + \frac{(\tilde{n}n_1)^{1/2}}{\sqrt{(x+n_0)^2+\tilde{n}n_1}}\Big]\right), \tag{S-4}$$

where $\tilde{n} = \Delta^2/(4\pi\hbar^2v^2)$ is the same as in the main text and $n_1 = \gamma_1^2/(4\pi\hbar^2v^2)$, and $N = 2$ is the spin degeneracy. We note that the large Berry flux per valley in dual-gated bilayer graphene yields a large maximal value of $\sigma_{xy}^{\rm pe} = 2Ne^2/h$. Eq. (S-4) yields a $\sigma_{xy}^{\rm pe}$ similar to that discussed in the main text, exhibiting a saturation behavior, and can also be tuned by carrier doping n_0.

In contrast to gapped single layer graphene, the characteristic density scale in dual-gated bilayer graphene is

$$n_* = \sqrt{n_1\tilde{n}}. \tag{S-5}$$

We note that $n_* > \tilde{n}$ since $\gamma_1 \gg \Delta$. However, large values of $\sigma_{xy}^{\rm pe}$ can still be achieved for small gap sizes in Eq. (S-4), and for relatively low photoexcited carrier density. Taking $\Delta = 10\,\text{meV}$ and $\gamma_1 = 0.38\,\text{eV}$, we find relatively low $n_* = 6.8\times10^{10}\,\text{cm}^{-2}$. Here we have used $v = 10^8\text{cm}\,s^{-1}$ as in the main text.

S1. Martin, I.; Blanter, Y. A.; Morpugo, A. F., *Phys. Rev. Lett.* **2008**, 100, 036804.
S2. Koshino, M., *New J. Phys* **2009**, 11, 095010.
S3. Zhang, F.; MacDonald, A. H.; Mele, E. J., *Proc. Natl. Acc. Sc.* **2013**, 110, 10546.
S4. Kuzmenko, A. B.; et al., *Phys. Rev. B* **2009**, 80, 165406.
S5. Zhang, Y.; et al., *Nature* **2009**, 459, 820.
S6. Shimazaki, Y.; et al., *Nat. Phys.* **2015**, 11, 1032.
S7. Sui, M.; et al., *Nat Phys.* **2015**, 11, 1027.
S8. Ju, L.; et al., *Nature* **2015**, 520, 650.